

Synergistic Modifications of Side Chains and End Groups in Small Molecular Acceptors for High Efficient Non-Fullerene Organic Solar Cells

Huanran Feng, Yuan-Qiu-Qiang Yi, Xin Ke, Yamin Zhang, Xiangjian Wan, Chenxi Li, and Yongsheng Chen*

Two new acceptor-donor-acceptor (A-D-A) type non-fullerene acceptors, O-NTIC and O-NTNC, using hexacyclic naphthalene (cyclopentadithiophene) (NT) as the electron-donating unit, and dicyanovinylindan-1-one (INCN) or phenyl-fused dicyanovinylindan-1-one (NINCN) as the electron-deficient unit, respectively, are synthesized. From the perspective of synthesis easiness and cost, para-alkoxy-phenyl is used as side chains of the NT core. It is worth noting that the introduction of para-alkoxy-phenyl unit could tune the molecular energy levels and lift the open-circuit voltage (V_{oc}). Compared with O-NTIC, the introduction of extended end-groups NINCN leads to a more ordered packing structure, much red-shifted absorption and enhanced electron mobility of O-NTNC. With polymer PBDB-T as the donor, the organic solar cell (OSC) devices obtain a decent power conversion efficiency (PCE) of 9.1% for O-NTIC and much improved PCE of 11.0% for O-NTNC, respectively. Moreover, with a polythiophene derivative named PDCBT as the donor material, the PDCBT:O-NTNC based device exhibits a PCE of 10.0%, among the highest PCEs for PDCBT devices. These results indicate that O-NTNC has great potential on the application for high performance and low-cost OSCs, and the extended end group NINCN as well as para-alkoxy-phenyl side chain substituted core could be promising units for the design of materials with high performance.

1. Introduction

Due to the attractive features of solution-processability, lightweight, flexibility, and low cost, organic solar cells (OSCs) have been regarded as a promising technology for clean and renewable energy conversion.^[1,2] In recent years, non-fullerene

(NF) electron acceptors, as a promising competitive alternative to fullerene derivative acceptors, emerged with much advantages of structural versatility, tunable optical, and electronic properties.^[3–5] OSCs with NF electron acceptors receive tremendous attention and have made significant progress benefiting from the rapid development of novel NF electron acceptors along with donor materials and device engineering.^[6–13]

In the design of NF acceptors, the prevalent and rather successful strategy is based on the acceptor-donor-acceptor (A-D-A) architecture which has been widely used for the design of donor materials in highly efficient fullerene-based OSCs. This is due to the easily tunable molecular energy levels, flexibility of the molecular structure, and easy purification.^[14–17] In the past two years, numerous new structural units for constructing A-D-A structures for NF small molecular acceptors have been employed and remarkable power conversion efficiency (PCE) over 13% of the OSCs based on the A-D-A type acceptors have been achieved.^[6–8,18]

Typically, the A-D-A structure based NF acceptors usually consist of three key components. The central fused donor units (D) could be used to decrease the reorganization energy and facilitate the π - π stacking, thus enhance the intrinsic charge mobility; the electron-deficient units (A) could be used for adjusting the lowest unoccupied molecular orbital (LUMO) energy levels, providing good light absorption and molecular stacking and improved electron mobilities, and the aromatic side-chains are usually used to tune the solubility required for solution processing and also ensure appropriate aggregation in the blend films with the polymer donor. Meanwhile, all the conjugated backbone, end groups and the side chains would have significant impact on the aggregation and intermolecular interactions in the active layer.^[19] To obtain higher performance NF acceptors, much effort have been devoted to chemical modification of end-deficient groups and side chains, as well as the donor core of the acceptors.^[13,20–26] Recently, several new end-deficient groups emerged and have been used for high-performance NF

H. Feng, Y.-Q.-Q. Yi, X. Ke, Y. Zhang, Prof. X. Wan, Prof. C. Li, Prof. Y. Chen
State Key Laboratory and Institute of Elemento-Organic Chemistry
The Centre of Nanoscale Science and Technology and Key Laboratory of Functional Polymer Materials
College of Chemistry
Nankai University
Tianjin 300071, China
E-mail: yschen99@nankai.edu.cn

 The ORCID identification number(s) for the author(s) of this article can be found under <https://doi.org/10.1002/solr.201800053>.

DOI: 10.1002/solr.201800053

acceptors, such as 2-(6-oxo-5,6-dihydro-4H-cyclopenta[b]thiophen-4-ylidene)malononitrile,^[27] CPTCN (2-(6-oxo-5,6-dihydro-4H-cyclopenta[c]thiophen-4-ylidene)malononitrile)^[28,29] and NINCN (2-(3-oxo-2,3-dihydro-1H-cyclopenta[b]naphthalen-1-ylidene)malononitrile),^[30–32] besides INCN (2-(3-oxo-2,3-dihydro-1H-inden-1-ylidene)malononitrile) and its derivatives which have been extensively studied.^[19,28,33] Among these new end-deficient units, NINCN with extended conjugated length show great potential for high performance OSCs due to its excellent ability of enhancing the light absorption and π - π stacking of the acceptor thus improving short-circuit current (J_{sc}), and especially fill factor (FF). On the other hand, manipulating the side chains of molecules in the NF-based OSCs has been demonstrated to be critically important for enhancing the photovoltaic performance.^[17,26,34–36] For example, using alkoxy-phenyl side chains was reported to be an easy and effective method to tune the molecular energy level thus achieving higher open-circuit voltage (V_{oc}).^[37] Meanwhile compared with alkyl-bromobenzene preparation using transition-metal catalyzed reaction, alkoxy-bromobenzene can be easily synthesized by a simple esterification reaction from cheap phenol starting material.^[35] Thus, introducing para-alkoxy-phenyl side chains into the NF acceptors could be a promising way for designing high performance acceptors.

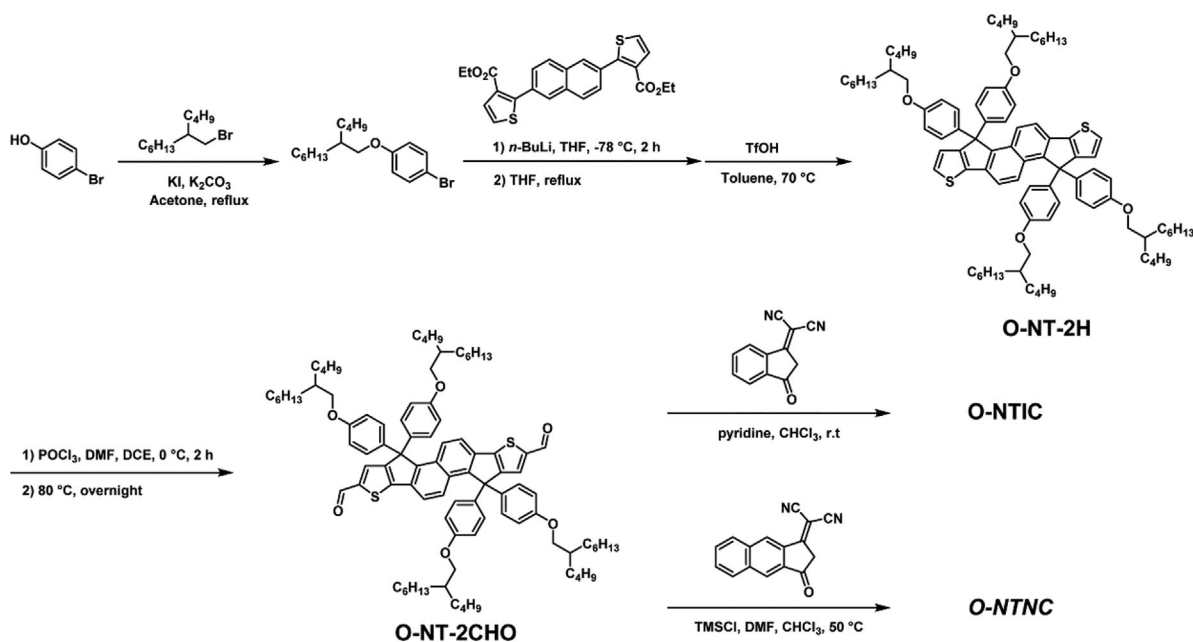
On the basis of these thoughts, two new NF acceptors (O-NTIC and O-NTNC) with INCN or NINCN as the end-deficient groups, and using NT substituted by para-alkoxy-phenyl side chains as the donor core unit, were designed and synthesized. The para-alkoxy-phenyl side chains not only provide another low-cost choice for design of small molecular acceptor, but also tune the energy levels of the molecules by elevating the LUMO level, benefit a high V_{oc} . Furthermore, introducing the extended end-groups NINCN for O-NTNC ensures the stronger π - π intermolecular stacking which leads to

a more ordered packing structure, much red-shifted absorption and enhanced electron mobility, thus a higher device performance can be expected.^[38] In the OSC devices using PBDB-T as the polymer donor, O-NTIC-based device obtains a PCE of 9.1% with a high V_{oc} of 0.978 V, a J_{sc} of 13.31 mA cm⁻² and FF of 69.9%. For O-NTNC-based device, a much higher PCE of 11.0% with a significantly improved J_{sc} of 15.98 mA cm⁻² and FF of 73.4%, a near 20% improvement in PCE comparing to O-NTIC-based device is achieved. These results indicate the extended end-groups as well as the para-alkoxy-phenyl side chains are promising units for enhancing PCE performance. Moreover, with a polythiophene derivative named PDCBT as donor material, the PDCBT:O-NTNC device exhibits a PCE of 10.0%, one of the highest for PDCBT based devices.

2. Results and Discussion

2.1. Synthesis and Characterization of the Molecules

The synthetic route of O-NTIC and O-NTNC are illustrated in **Scheme 1**. 1-bromo-4-(2'-butyloctyloxy)benzene was synthesized by etherification reaction. Diethyl 2,2'-(naphthalene-2,6-diyl)bis(thiophene-3-carboxylate) was first prepared according to our previous reported approach.^[39] Then ((2-butyloctyl)oxy)phenyl side chains was linked to it and giving the tertiary alcohol, which could be used in the next step without purification. The π -fused ring core (O-NT-H) was synthesized by intramolecular Friedel-Crafts reaction of the tertiary alcohol in the presence of trifluoromethanesulfonic acid. The dialdehyde compound (O-NT-2CHO) was prepared by the Vilsmeier-Haack reaction with POCl₃ and DMF (*N,N*-dimethylformamide) as a light-yellow solid. The desired O-NTIC and O-NTNC were then obtained by the Knoevenagel condensation of the dialdehyde



Scheme 1. The synthetic routes to O-NTIC and O-NTNC.

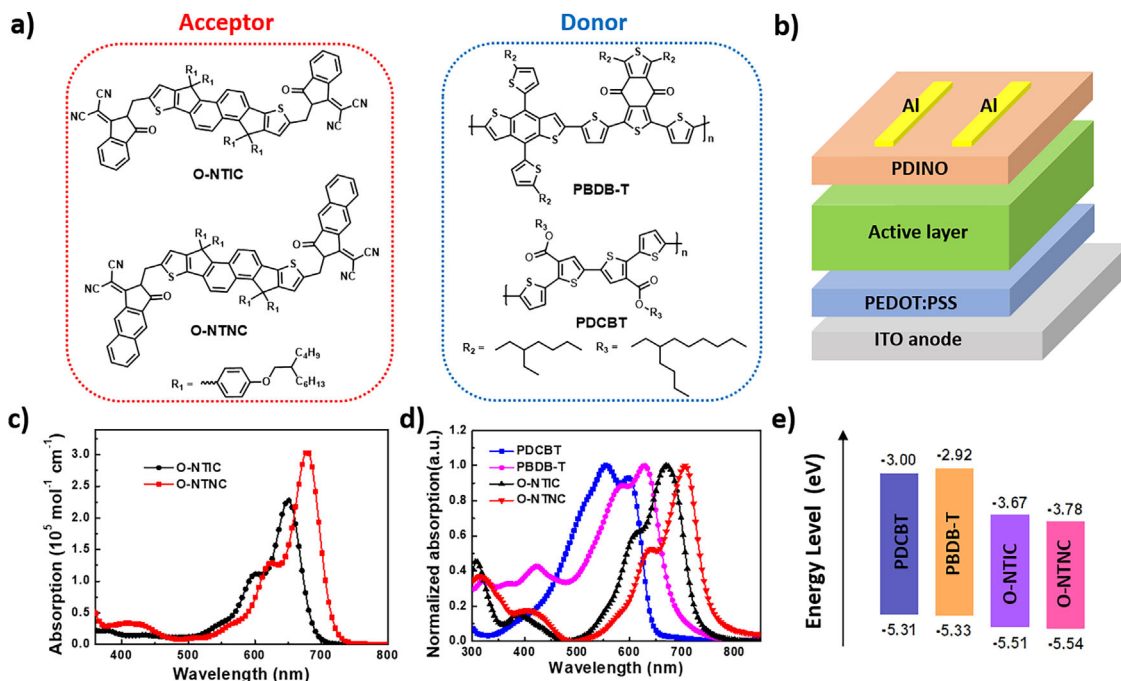


Figure 1. a) Chemical structures of donor polymers (PBDB-T and PDCBT) and acceptors (O-NTIC, O-NTNC). b) The device structure used in this study. UV-vis absorption spectra of (c) acceptors in chloroform solution and (d) the acceptors and donors (PBDB-T and PDCBT) as film. e) Energy level diagram of acceptors and donors.

O-NT-CHO with INCN or NINCEN. The thermal stability of the two molecules was evaluated by thermogravimetric analysis (TGA), as shown in Figure S1 in the Supporting Information (SI). They both show good thermal stability and the decomposition temperature at 5% weight loss are 356 and 376 °C for O-NTIC and O-NTNC, respectively.

2.2. Photophysical and Electrochemical Properties

The ultraviolet-visible (UV-Vis) absorption spectra of O-NTIC and O-NTNC in chloroform solution and as film are shown in Figure 1c and d, respectively. The corresponding data are summarized in Table 1. The maximum absorption peak (λ_{\max}) of O-NTIC and O-NTNC in solution are located at 650 nm with the molar extinction coefficient of $2.5 \times 10^5 \text{ M}^{-1} \text{ cm}^{-1}$ and 679 nm with $3.0 \times 10^5 \text{ M}^{-1} \text{ cm}^{-1}$, respectively. The λ_{\max} peaks of O-NTIC and O-NTNC films are located at 671 and 706 nm, respectively. Meanwhile, the extinction coefficient of O-NTNC in solid film is also much higher than that of O-NTIC. Compared with O-NTIC, O-NTNC exhibits redshifted and stronger optical absorption due

to the extended effective conjugated length which achieved by the larger end-groups.^[40] As can be seen from Figure S2, in Supporting Information, the temperature-dependent absorption spectra of O-NTIC and O-NTNC in chloroform both have slight and neglectable aggregation in solution, thus a larger redshift in the absorption spectrum of O-NTNC from solution to film state can be attributed to the much stronger π - π intermolecular interactions formed in the O-NTNC film. Thus, O-NTNC owns a lower optical bandgap (E_g^{opt}) of 1.64 eV than 1.70 eV of O-NTIC. Note, for O-NTIC with alkoxy-phenyl side chains, it has only slightly increased optical band gap of 0.02 eV compared with our previous acceptor (NTIC) with alkyl-phenyl side chains,^[39] thus the impact on J_{sc} can be minimized.

The frontier molecular orbital energy levels of O-NTIC and O-NTNC were determined by electrochemical cyclic voltammetry (CV) referenced to the energy level of Fc/Fc⁺ (−4.8 eV below the vacuum level) (Figure S3, in Supporting Information). Compared with O-NTIC, O-NTNC shows a slightly deeper lowest unoccupied molecular orbital (LUMO) level (−3.67 eV vs. −3.78 eV) and similar highest occupied molecular orbital (HOMO) level (−5.51 eV with −5.54 eV), which is consistent

Table 1. Optical and electrochemical data of O-NTIC and O-NTNC.

Comp.	$\lambda_{\max}^{\text{sol}}$ [nm]	$\epsilon_{\max}^{\text{sol}}$ [$\text{M}^{-1} \text{ cm}^{-1}$]	$\lambda_{\max}^{\text{film}}$ [nm]	$\epsilon_{\max}^{\text{film}}$ [10^5 cm^{-1}]	$\lambda_{\text{edge}}^{\text{film}}$ [nm]	E_g^{opt} [eV] ^{a)}	HOMO [eV] ^{b)}	LUMO [eV] ^{b)}	E_g^{cv} [eV] ^{c)}
O-NTIC	650	2.2×10^5	671	0.79	729	1.70	−5.51	−3.67	1.84
O-NTNC	679	3.0×10^5	706	1.23	756	1.64	−5.54	−3.78	1.76

^{a)}The optical band gap estimated from the absorption onset; ^{b)} $E_{\text{HOMO}} = -(4.80 + E_{\text{ox}}^{\text{onset}})$, $E_{\text{LUMO}} = -(4.80 + E_{\text{re}}^{\text{onset}})$; ^{c)}Electrochemical bandgap obtained from $E_{\text{LUMO}} - E_{\text{HOMO}}$.

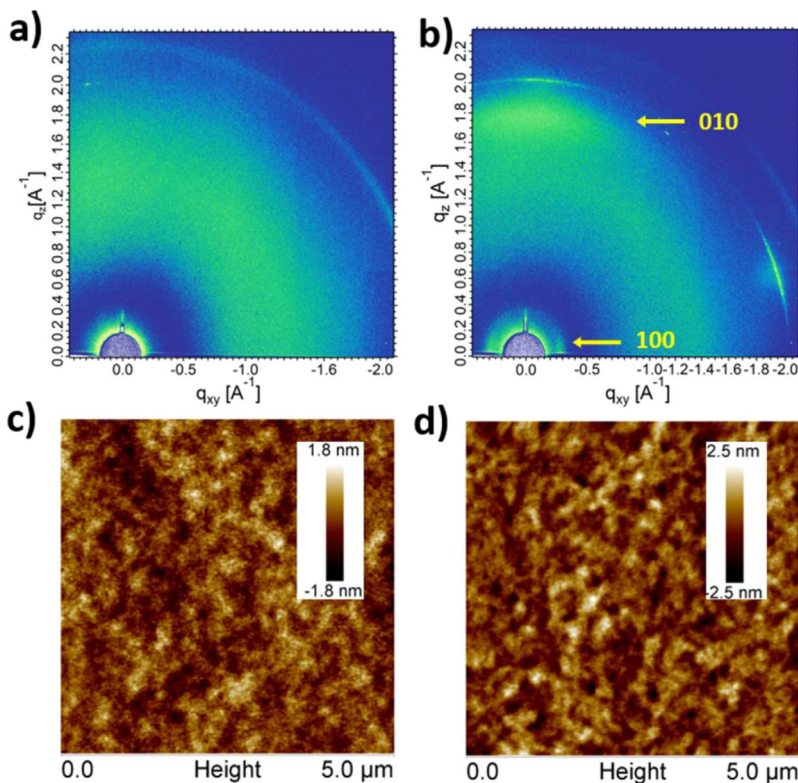


Figure 2. 2D-GIXD patterns for pure films of (a) O-NTIC and (b) O-NTNC. AFM height images of (c) O-NTIC and (d) O-NTNC films.

with the results obtained from theoretical calculations as presented in Figure S4, in Supporting Information. On the other hand, we note that the replacement of alkyl-phenyl groups by para-alkoxy-phenyl groups elevated the HOMO and LUMO level of O-NTIC by 0.09 and 0.07 eV compared to that of NTIC, respectively. Since V_{oc} is closely related to the band gap between the LUMO of the acceptor material and the HOMO of the donor polymer in the active layers, the upshifted LUMO levels of O-NTIC could lead to an improved V_{oc} .

The molecular ordering of O-NTIC and O-NTNC neat films were investigated by two-dimensional grazing-incidence X-ray diffraction (2D-GIXD). As shown in Figure 2, no clear X-ray diffraction peaks were observed for O-NTIC, indicating the amorphous structure of the O-NTIC film. With the extended end-groups, O-NTNC exhibited a strong lamellar (100) diffraction peak (at 0.26 \AA^{-1}) with an interlamellar distance of 24.1 \AA in the in-plane (IP) direction and an obvious π - π stacking (010) diffraction peak (1.77 \AA^{-1}) in the out-of-plane direction with a d-spacing of 3.5 \AA . These suggest the high crystallinity and preferential face-on packing of O-NTNC. A larger surface roughness root mean square (RMS) of 0.63 nm for O-NTNC over 0.45 nm for O-NTIC plus the 2D-GIXD result further indicate the high crystalline feature in O-NTNC film. In addition, we investigated the electron mobilities of O-NTIC and O-NTNC by employing space-charge-limited current (SCLC) method (Figure S6, in Supporting Information). O-NTNC shows higher electron mobilities ($4.06 \times 10^{-4} \text{ cm}^2 \text{ V}^{-1} \text{ s}^{-1}$) than that of O-NTIC ($1.27 \times 10^{-4} \text{ cm}^2 \text{ V}^{-1} \text{ s}^{-1}$),

which can be mainly attributed to the better packing and more preference on face-on orientation of O-NTNC as seen in 2D-GIXD. These results indicate that the extended end groups in O-NTNC ensure a stronger π - π intermolecular stacking and charge transport which will benefit effective carrier transport and reduce carrier recombination when used as electron acceptor.

2.3. Photovoltaic Properties

To investigate the photovoltaic performance of the two new acceptors, we fabricated the OSCs based on PBDB-T as donor and O-NTIC or O-NTNC as acceptor with a conventional device configuration: ITO/PEDOT:PSS/active layer/PDINO/Al, where PDINO is an efficient cathode interlayer developed by Li et al.^[41] The detailed device optimization processes are described in the Tables S1–S3, in Supporting Information, including different donor/acceptor weight ratios and the effects of solvent additives. When utilizing chlorobenzene as the processing solvent, the optimal D/A weight ratio for both blends is 1:0.8. And further improved performance were obtained by adding a tiny amount of DIO as the additive. The current-density–voltage (J - V) curves of the PSCs based on PBDB-T:O-NTIC and PBDB-T:

O-NTNC with the optimal photovoltaic performance are shown in Figure 3a, and the corresponding photovoltaic parameters are listed in Table 2. The optimal OSC based on PBDB-T:O-NTIC showed a PCE of 9.1% with a improved V_{oc} of 0.978 V compared with NTIC-based device,^[39] benefitting from the relatively high-lying LUMO energy levels of O-NTIC. After introducing the extended end-group NINIC, the O-NTNC-based devices showed a further improved PCE of 11.0% with a V_{oc} of 0.942 V , a J_{sc} of 15.98 mA cm^{-2} , and an FF of 73.4%. Compared with the O-NTIC-based device, though the O-NTNC-based device showed a slightly lower V_{oc} , it exhibited a significantly improved J_{sc} and FF, thus a nearly 20% promotion in PCEs was achieved. In addition, to investigate generality and the potential for low-cost OSCs of O-NTNC, we further used a polythiophene derivative named PDCBT as the donor material to fabricate OSC devices. As shown in Figure S9, in Supporting Information, the PDCBT:O-NTNC based device exhibited a PCE of 10.0%, one of the highest PCEs for polythiophene system. This indicates the great potential of O-NTNC on the application for high performance and low-cost OSCs.

The external quantum efficiency (EQE) spectra of the PBDB-T:O-NTIC and PBDB-T:O-NTNC-based devices were displayed in Figure 3b. The O-NTNC-based devices show broader photoresponse and higher EQE value which contributes to the higher J_{sc} . In addition, the EQE values in the range of 650–750 nm (mostly contributed by acceptor) are significantly increased for the O-NTNC-based device, which can be partially attributed to

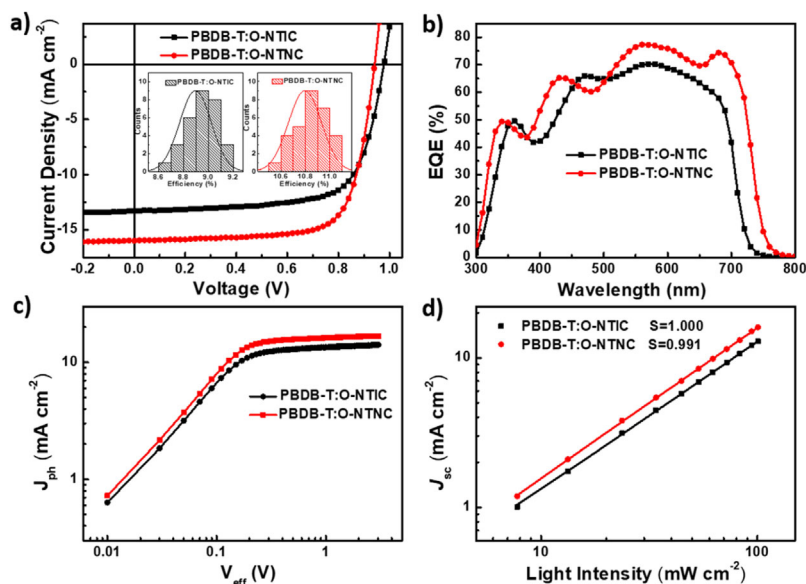


Figure 3. a) Current density–voltage (J – V) curves for the devices based on O-NTIC and O-NTNC at optimized conditions under the illumination of AM 1.5G (100 mW cm^{-2}); the inset shows the histograms of the PCE counts for 30 devices. b) EQE curves for the O-NTIC and O-NTNC based OSC devices. c) J_{ph} versus V_{eff} and d) light intensity (P) dependence of J_{sc} for the optimized devices.

the stronger optical absorption of O-NTNC. For both devices, the integrated current density values calculated from EQE spectra ($J_{calc.}$) matched well with those obtained from the J – V measurements. To investigate the charge transfer properties in the blend films, photoluminescence (PL) quenching spectra were measured. As shown in Figure S8, in Supporting Information, the PL intensities of pure donor PBDB-T and O-NTIC or O-NTNC are significantly quenched in each blend film, and the higher quenching efficiency of O-NTNC (92%) than that of O-NTIC (89%) suggesting more efficient charge transfer among the D/A interfaces for PBDB-T:O-NTNC blend films. These are consistent with the higher EQE and J_{sc} values of the related devices.

The carrier transport mobility of the blend films based on the two new acceptors were also examined by using SCLC method (Figure S7, in Supporting Information). Relative to the PBDB-T:O-NTIC blend film (hole mobility, $\mu_h = 1.54 \times 10^{-4} \text{ cm}^2 \text{ V}^{-1} \text{ s}^{-1}$; electron mobility, $\mu_e = 8.27 \times 10^{-5} \text{ cm}^2 \text{ V}^{-1} \text{ s}^{-1}$; $\mu_h/\mu_e = 1.9$), the PBDB-T:O-NTNC film possesses higher mobilities ($\mu_h = 2.55 \times 10^{-4} \text{ cm}^2 \text{ V}^{-1} \text{ s}^{-1}$; $\mu_e = 1.69 \times 10^{-4} \text{ cm}^2 \text{ V}^{-1} \text{ s}^{-1}$) and

also more symmetric hole/electron mobilities ($\mu_h/\mu_e = 1.5$), which are partly responsible for the higher J_{sc} and FF.^[42]

Photogenerated current density (J_{ph}) versus effective voltage (V_{eff}) curves were plotted to investigate the exciton dissociation and charge collection properties of the two OSCs with O-NTIC and O-NTNC as acceptor. As shown in Figure 3c, J_{ph} values for both devices are saturated (J_{sat}) at 2 V, suggesting that charge recombination in both devices is minimized at higher voltage.^[43] Under short circuit conditions, The J_{ph}/J_{sat} ratio for O-NTIC- and O-NTNC-based devices is calculated to be 95 and 96%, respectively, implying the overall exciton dissociation and charge collection processes all are quite efficient for the O-NTIC and O-NTNC-based OSCs. The light-intensity (P) dependence of J_{sc} was also measured to further study the charge combination in the devices.^[44]

As shown in Figure 3d, by fitting the relationship of photocurrent and light intensity, the power-law exponents of the equation J_{ph} for the O-NTNC- and O-NTIC-based devices are 1.00 and 0.99, respectively, suggesting that the bimolecular recombination is efficiently suppressed in both devices.

2.4. Morphology Characterization

To explore the microscopic morphology, detailed investigations of the blend films were conducted by atomic force microscopy (AFM), transmission electron microscopy (TEM) and 2D-GIXD. As shown in Figure 4a and b, both blend films exhibit good miscibility of the donor and acceptor components, with the RMS for the PBDB-T:O-NTNC blends and PBDB-T:O-NTIC blends of 2.98 and 3.07 nm, respectively. Compared with PBDB-T:O-NTNC blend film, PBDB-T:O-NTNC based film shows more defined fibrous and continuous interpenetrating structure in the TEM images (Figure 4c and d), which will benefit exciton dissociation and charge transport. The 2D-GIXD measurement was used to investigate the molecular packing of the blend films. As shown in Figure 4e–h, the 2D-GIXD diffraction of PBDB-T:O-NTIC blends was dominated by the polymer diffraction signals with a (100) peak at 0.28 \AA^{-1} in plane and a π – π stacking (010) peak out of plane at 1.69 \AA^{-1} , and there is no clear peak from the

Table 2. The optimized photovoltaic parameters of the devices based on PBDB-T:O-NTIC and PBDB-T:O-NTNC blend under the illumination of AM 1.5G (100 mW cm^{-2}).

Blend	V_{oc} [V]	J_{sc} [mA cm^{-2}]	J_{calc}^a (mA cm^{-2})	FF [%]	PCE ^b [%]
PBDB-T:O-NTIC	0.978 (0.972 ± 0.006)	13.31 (12.95 ± 0.50)	13.10	69.9 (68.6 ± 1.5)	9.1 (8.9 ± 0.2)
PBDB-T:O-NTNC	0.942 (0.936 ± 0.008)	15.98 (15.60 ± 0.40)	15.68	73.4 (72.5 ± 1.8)	11.0 (10.8 ± 0.2)
PDCBT:O-NTNC	0.940 (0.936 ± 0.006)	15.51 (14.5 ± 0.20)	14.93	(66.3 ± 1.6)	10.0 (9.8 ± 0.2)

^aValues calculated from EQE; ^bThe average PCE value was calculated from 30 devices.

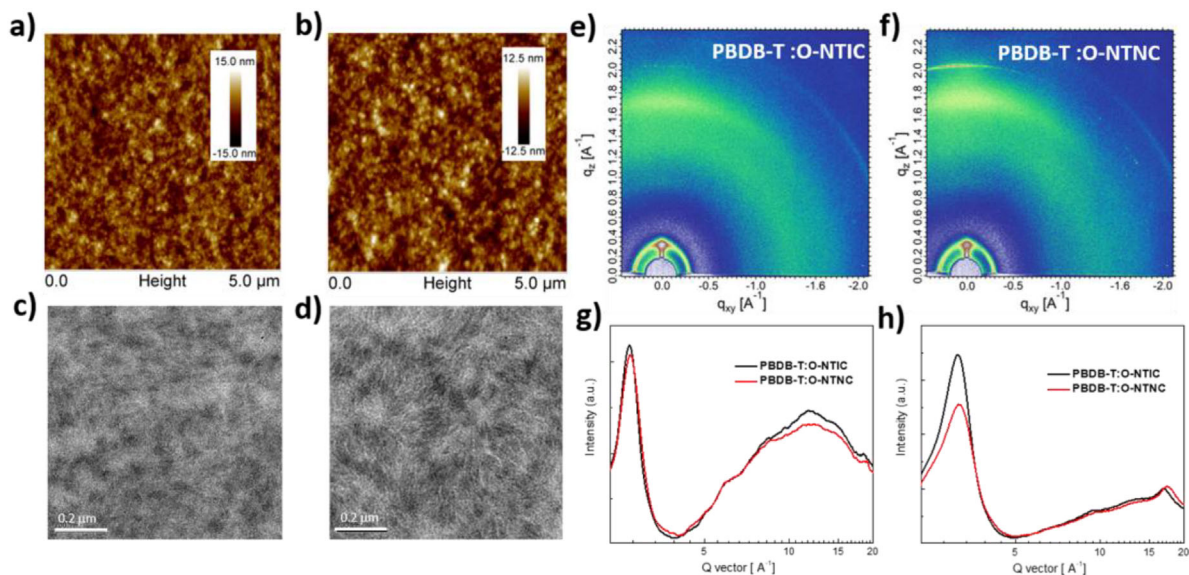


Figure 4. AFM height and TEM images of the blend films based on (a,c) PBDB-T:O-NTIC and (b,d) PBDB-T:O-NTNC. 2D GIXD patterns of the (e) PBDB-T:O-NTIC and (f) PBDB-T:O-NTNC films. The (g) in-plane and (h) out-of-plane line cuts of the corresponding 2D-GIXD patterns.

acceptor O-NTIC. For the PBDB-T:O-NTNC blend film, the original (010) peak out of plane at 1.69 \AA^{-1} has been broadened with the q values of the peak positions shift to 1.74 \AA^{-1} due to O-NTNC, demonstrating the much stronger π - π stacking than O-NTIC in the blend films as well as in the neat film, which is one of the keys for the higher device performance. The above results demonstrated the extended end-groups could significantly improve the morphology of the blend films, owing to the enhanced crystallinity of O-NTNC which can break away from the intimate mixtures with polymer donor.

3. Conclusion

In summary, two new small-molecule acceptors O-NTIC and O-NTNC based on hexacyclic naphthalene (cyclopentadithiophene) core were designed and synthesized. The alkoxy-phenyl side chains replacing alkyl-phenyl ones were used for the easier synthesis and scalability and it is found the replacement could tune the energy levels of the molecules and leads to a higher V_{oc} . By introducing the extended end group NINCN, O-NTNC possessed larger π -conjugation with stronger intermolecular π - π stacking and exhibited redshifted optical absorption, higher and balanced charge transport, as well as better nanoscale interpenetrating morphology compared with O-NTIC with the INCN as end-group. As a result, the device based on PBDB-T:O-NTNC exhibited a PCE of 11.0% with a V_{oc} of 0.978 V, a J_{sc} of 15.98 mA cm^{-2} , and an FF of 73.4%, a near 20% boost in PCE compared with 9.1% of PBDB-T:O-NTIC based device. In addition, when a polythiophene derivative PDCBT was used as the donor material, the resulting O-NTNC-based PSCs exhibited a PCE of 10.0%, one of the highest PCEs for polythiophene system and exhibiting potential for highly efficient and low-cost OSCs for practical applications. These results indicate that O-NTNC is a promising small molecular

acceptor for non-fullerene OSCs and the extended end-groups as well as para-alkoxy-phenyl side chains substituted core could be promising units to further improve the photovoltaic performance of the donor and acceptor materials for high efficiency OSCs.

Supporting Information

Supporting Information is available from the Wiley Online Library or from the author.

Acknowledgements

H. Feng and Y.-Y.-Q Yi contributed equally to this work. The authors gratefully acknowledge the financial support from National Natural Science Foundation of China (NSFC) (51773095, 91633301), the Ministry of Science and Technology of China (2014CB643502) and Tianjin City (17JCQJC44500, 17CZDJC31100), 111 Project (B12015). The authors gratefully thank the beam time and technical supports provided by BL14B1 GIWAXS beamline at Shanghai Synchrotron Radiation facility (SSRF).

Conflict of Interest

The authors declare no conflict of interest.

Keywords

acceptor-donor-acceptor structure, extended end-groups, organic solar cells, para-alkoxy-phenyl side chain, small molecular acceptors

Received: February 22, 2018
Revised: March 21, 2018
Published online: May 2, 2018

- [1] G. Yu, J. Gao, J. C. Hummelen, F. Wudl, A. J. Heeger, *Science* **1995**, 270, 1789.
- [2] G. Li, R. Zhu, Y. Yang, *Nat. Photonics* **2012**, 6, 153.
- [3] C. B. Nielsen, S. Holliday, H. Y. Chen, S. J. Cryer, I. McCulloch, *Acc. Chem. Res.* **2015**, 48, 2803.
- [4] S. Li, Z. Zhang, M. Shi, C. Z. Li, H. Chen, *Phys. Chem. Chem. Phys.* **2017**, 19, 3440.
- [5] Y. Lin, X. Zhan, *Acc. Chem. Res.* **2016**, 49, 175.
- [6] Z. Fei, F. D. Eisner, X. Jiao, M. Azzouzi, J. A. Rohr, Y. Han, M. Shahid, A. S. R. Chesman, C. D. Easton, C. R. McNeill, T. D. Anthopoulos, J. Nelson, M. Heeney, *Adv. Mater.* **2018**, 30, 1705209.
- [7] Y. Cui, H. Yao, B. Gao, Y. Qin, S. Zhang, B. Yang, C. He, B. Xu, J. Hou, *J. Am. Chem. Soc.* **2017**, 139, 7302.
- [8] W. Zhao, S. Li, H. Yao, S. Zhang, Y. Zhang, B. Yang, J. Hou, *J. Am. Chem. Soc.* **2017**, 139, 7148.
- [9] X. L. Shi, L. J. Zuo, S. B. Jo, K. Gao, F. Lin, F. Liu, A. K. Y. Jen, *Chem. Mater.* **2017**, 29, 8369.
- [10] T. Li, S. Dai, Z. Ke, L. Yang, J. Wang, C. Yan, W. Ma, X. Zhan, *Adv. Mater.* **2018**, 30, 1705969.
- [11] Z. Luo, H. Bin, T. Liu, Z. G. Zhang, Y. Yang, C. Zhong, B. Qiu, G. Li, W. Gao, D. Xie, K. Wu, Y. Sun, F. Liu, Y. Li, C. Yang, *Adv. Mater.* **2018**, 30, 1706124.
- [12] H.-H. Gao, Y. Sun, X. Wan, B. Kan, X. Ke, H. Zhang, C. Li, Y. Chen, *Sci. China Mater.* **2017**, 60, 819.
- [13] B. Kan, J. Zhang, F. Liu, X. Wan, C. Li, X. Ke, Y. Wang, H. Feng, Y. Zhang, G. Long, R. H. Friend, A. A. Bakulin, Y. Chen, *Adv. Mater.* **2018**, 30, 1704904.
- [14] Y. Chen, X. Wan, G. Long, *Acc. Chem. Res.* **2013**, 46, 2645.
- [15] H. Yao, Y. Cui, R. Yu, B. Gao, H. Zhang, J. Hou, *Angew. Chem. Int. Ed.* **2017**, 56, 3045.
- [16] Y. Wu, H. Bai, Z. Wang, P. Cheng, S. Zhu, Y. Wang, W. Ma, X. Zhan, *Energy Environ. Sci.* **2015**, 8, 3215.
- [17] Y. Yang, Z. G. Zhang, H. Bin, S. Chen, L. Gao, L. Xue, C. Yang, Y. Li, *J. Am. Chem. Soc.* **2016**, 138, 15011.
- [18] Z. Xiao, X. Jia, L. Ding, *Sci. Bull.* **2017**, 62, 1562.
- [19] N. Liang, W. Jiang, J. Hou, Z. Wang, *Mater. Chem. Front.* **2017**, 1, 1291.
- [20] S. Li, L. Ye, W. Zhao, S. Zhang, S. Mukherjee, H. Ade, J. Hou, *Adv. Mater.* **2016**, 28, 9423.
- [21] N. Qiu, H. Zhang, X. Wan, C. Li, X. Ke, H. Feng, B. Kan, H. Zhang, Q. Zhang, Y. Lu, Y. Chen, *Adv. Mater.* **2017**, 29, 1604964.
- [22] S. Dai, F. Zhao, Q. Zhang, T. K. Lau, T. Li, K. Liu, Q. Ling, C. Wang, X. Lu, W. You, X. Zhan, *J. Am. Chem. Soc.* **2017**, 139, 1336.
- [23] Y. Yang, Z. G. Zhang, H. Bin, S. Chen, L. Gao, L. Xue, C. Yang, Y. Li, *J. Am. Chem. Soc.* **2016**, 138, 15011.
- [24] S. Feng, C. e. Zhang, Y. Liu, Z. Bi, Z. Zhang, X. Xu, W. Ma, Z. Bo, *Adv. Mater.* **2017**, 29, 1703527.
- [25] H. Bin, L. Gao, Z. G. Zhang, Y. Yang, Y. Zhang, C. Zhang, S. Chen, L. Xue, C. Yang, M. Xiao, Y. Li, *Nat. Commun.* **2016**, 7, 13651.
- [26] Y. Lin, F. Zhao, Q. He, L. Huo, Y. Wu, T. C. Parker, W. Ma, Y. Sun, C. Wang, D. Zhu, A. J. Heeger, S. R. Marder, X. Zhan, *J. Am. Chem. Soc.* **2016**, 138, 4955.
- [27] H. Yao, L. Ye, J. Hou, B. Jang, G. Han, Y. Cui, G. M. Su, C. Wang, B. Gao, R. Yu, H. Zhang, Y. Yi, H. Y. Woo, H. Ade, J. Hou, *Adv. Mater.* **2017**, 29, 1700254.
- [28] D. Xie, T. Liu, W. Gao, C. Zhong, L. Huo, Z. Luo, K. Wu, W. Xiong, F. Liu, Y. Sun, C. Yang, *Sol. RRL* **2017**, 1, 1700044.
- [29] Z. Zhang, L. Feng, S. Xu, J. Yuan, Z.-G. Zhang, H. Peng, Y. Li, Y. Zou, *J. Mater. Chem. A* **2017**, 5, 11286.
- [30] S. Li, L. Ye, W. Zhao, X. Liu, J. Zhu, H. Ade, J. Hou, *Adv. Mater.* **2017**, 29, 1704051.
- [31] H. Feng, N. Qiu, X. Wang, Y. Wang, B. Kan, X. Wan, M. Zhang, A. Xia, C. Li, F. Liu, H. Zhang, Y. Chen, *Chem. Mater.* **2017**, 29, 7908.
- [32] R. Li, G. Liu, M. Xiao, X. Yang, X. Liu, Z. Wang, L. Ying, F. Huang, Y. Cao, *J. Mater. Chem. A* **2017**, 5, 23926.
- [33] F. Yang, C. Li, W. Lai, A. Zhang, H. Huang, W. Li, *Mater. Chem. Front.* **2017**, 1, 1389.
- [34] Z. Luo, Y. Zhao, Z. G. Zhang, G. Li, K. Wu, D. Xie, W. Gao, Y. Li, C. Yang, *ACS Appl. Mater. Interfaces* **2017**, 9, 34146.
- [35] Z. Zhang, L. Feng, S. Xu, Y. Liu, H. Peng, Z. G. Zhang, Y. Li, Y. Zou, *Adv. Sci.* **2017**, 4, 1700152.
- [36] Y. Ma, M. Zhang, Y. Yan, J. Xin, T. Wang, W. Ma, C. Tang, Q. Zheng, *Chem. Mater.* **2017**, 29, 7942.
- [37] M. Zhang, X. Guo, W. Ma, S. Zhang, L. Huo, H. Ade, J. Hou, *Adv. Mater.* **2014**, 26, 2089.
- [38] B. Gao, H. Yao, B. Jang, J. Zhu, R. Yu, Y. Cui, F. Wang, J. Hou, H. Y. Woo, J. Hou, *J. Mater. Chem. A* **2018**, 6, 2664.
- [39] Y.-Q. Yi, H. Feng, M. Chang, H. Zhang, X. Wan, C. Li, Y. Chen, *J. Mater. Chem. A* **2017**, 5, 17204.
- [40] B. Kobin, L. Grubert, S. Blumstengel, F. Henneberger, S. Hecht, *J. Mater. Chem.* **2012**, 22, 4383.
- [41] Z.-G. Zhang, B. Qi, Z. Jin, D. Chi, Z. Qi, Y. Li, J. Wang, *Energy Environ. Sci.* **2014**, 7, 1966.
- [42] H. Zhou, Y. Zhang, J. Seifert, S. D. Collins, C. Luo, G. C. Bazan, T.-Q. Nguyen, A. J. Heeger, *Adv. Mater.* **2013**, 25, 1646.
- [43] M. Lenes, M. Morana, C. J. Brabec, P. W. M. Blom, *Adv. Funct. Mater.* **2009**, 19, 1106.
- [44] C. M. Proctor, M. Kuik, T.-Q. Nguyen, *Prog. Polym. Sci.* **2013**, 38, 1941.